Size-dependent structure of CdSe nanoclusters formed after ion implantation in MgO

van Huis, MA; van Veen, A; Schut, H; Eijt, SWH; Kooi, BJ; De Hosson, JTM

Published in:
Acta Materialia

DOI:
10.1016/j.actamat.2004.11.023

Publication date:
2005

Available online at www.sciencedirect.com
SCIENCE DIRECT®
Acta Materialia 53 (2005) 1305–1311
Acta MATERIALIA
www.actamat-journals.com

Size-dependent structure of CdSe nanoclusters formed after ion implantation in MgO

M.A. van Huis [a,*], A. van Veen [a,✠], H. Schut [a], S.W.H. Eijt [a], B.J. Kooi [b], J.Th.M. De Hosson [b]

[a] *Interfaculty Reactor Institute, Delft University of Technology, Mekelweg 15, NL 2629 JB Delft, The Netherlands*
[b] *Department of Applied Physics, Materials Science Centre and The Netherlands Institute for Metals Research, University of Groningen, Nijenborgh 4, NL 9747 AG Groningen, The Netherlands*

Received 18 August 2004; received in revised form 12 November 2004; accepted 16 November 2004
Available online 18 December 2004

Abstract

The band gap as well as the optical and structural properties of semiconductor CdSe nanoclusters change as a function of the nanocluster size. Embedded CdSe nanoclusters in MgO were created by means of sequential Cd and Se ion implantation followed by thermal annealing. Changes during annealing were monitored using optical absorption and positron annihilation spectroscopy. High-resolution TEM on cross-sections after annealing at a temperature of 1300 K showed that clusters with a size below 5 nm have the high-pressure rock-salt structure and are in a cube-on-cube orientation relation with MgO, whereas clusters larger than 5 nm adopt the stable wurtzite crystal structure and were observed in two different orientation relations with MgO.

Keywords: Phase transformations; Precipitation; High-resolution electron microscopy; Positron annihilation; Compound semiconductors

1. Introduction

Optical, electrical and structural properties of nanoclusters vary as a function of size, offering unique opportunities to tailor material properties for future use in applications. Semiconductor nanoclusters are particularly interesting because, in contrast to metallic nanoclusters, the electronic and optical properties start to change already below a size of ~20 nm. Compared to the bulk properties of semiconductors, semiconductor nanocrystals exhibit uncommon crystal structures, lower melting temperatures and changes in the width of the band gap [1–5]. A crucial feature of nanoclusters is the large fraction of surface atoms. The first few atomic layers at the outside of the nanocluster will have properties different from the interior of the nanocluster due to surface reconstruction, presence of defects, other charge carriers and bending of electron bands. In order to passivate the surface area nanoclusters should be embedded in a host with a large band gap and similar structural properties. Ion implantation into ceramic oxides is a practical method of creating embedded, electronically passivated semiconductor nanoclusters [6]. An interesting candidate is MgO that has a high melting temperature (>3000 K) and a large band gap of 7.8 eV. Furthermore, it is optically transparent so that the optical properties of the nanoclusters (and of the composite material) can still be investigated. Apart from Si and Ge, most semiconductors are compounds and therefore require co-implantation of the elements constituting the semiconductor. One of the semiconductor cluster

* Corresponding author. Present address: Kavli Institute of Nanoscience, Delft University of Technology, Rotterdamseweg 137, NL 2628 AL Delft, The Netherlands. Tel.: + 31 15 2782054; fax: + 31 15 2786730.
E-mail address: m.a.vanhuis@tnw.tudelft.nl (M.A. van Huis).
✠ Deceased January 3, 2004.

1359-6454/$30.00
doi:10.1016/j.actamat.2004.11.023

systems that received much attention is CdSe [3–5]. The band gap of CdSe nanoclusters increases with decreasing cluster size, e.g., the band gap of CdSe clusters with a size of 2 nm is 2.5 eV while the band gap of bulk CdSe is 1.8 eV. In addition, phase transitions occur when the cluster size changes [7].

In this paper, the formation of CdSe nanoclusters in MgO by sequential Cd and Se ion implantation is discussed. The defect evolution during the annealing treatment is monitored with the aid of three complementary techniques: optical absorption spectroscopy, transmission electron microscopy (TEM) and positron annihilation spectroscopy (PAS). Besides the well known techniques suitable to observe precipitates and nanocavities (such as TEM, including all the analytical tools added to the electron microscope in the last decade) the less known positron annihilation technique has been used in this work to study nano-sized precipitates. The positron is the antiparticle of the electron. Hence, it has the same mass and the same spin (1/2), but opposite charge and magnetic moment. Positrons are unstable in matter where they annihilate with electrons predominantly via 2γ decay. The two photons are emitted collinearly in opposite directions and carry an energy of 511 keV each. The emission of more photons is also possible, but the probability of such an event is small. If the momentum of the electron-positron pair is non-zero, there is a shift of the energy of the photons from the value of $E_0 = m_0c^2$ ($\sim$511 keV), caused by the component of the momentum parallel to the direction of γ-ray emission (the longitudinal component). Here m_0 is the mass of the electron (which is equal to the mass of the positron) and c is the speed of light. One photon receives an energy of $E_0 - \delta E$, the other $E_0 + \delta E$. The so-called Doppler shift can be expressed as $\delta E = cp_z/2$, where p_z is the longitudinal component of the momentum of the electron-positron pair. Since one half of the electrons moves towards the photon detector while the other half moves away from it, the energy shift results in a Doppler broadening of the 511 keV photo-peak by several keVs, which can be measured by Ge-detectors. Consequently, the momentum distribution of the electrons in the material is reflected in the shape of the Doppler broadened 511 keV peak.

One can derive valuable information from the Doppler broadened peak by defining regions of interest. The low-momentum central part of the peak (small Doppler shift) corresponds to annihilations of positrons with valence or conduction electrons, and the high-momentum tails of the peak (large Doppler shift) correspond to annihilations with more tightly bound electrons, e.g., core electrons. The shape of the peak is characterized by the so-called S parameter and is defined as the area under the central part of the 511 keV peak, divided by the total area under the peak. Because a positron is a positively charged particle that is repelled by nuclei, it is very sensitive to the presence of open volume on an atomic scale. Positrons that are trapped in open volume defects mainly annihilate with valence or conduction electrons (contributing to the center of the profile), and therefore a high value of S signals the presence of vacancies and other open-volume defects, whereas a 'defect-free' sample will show a low value of the S parameter. The S parameter is thus very useful for monitoring the presence of defects in a material.

Because of this strong preference of positrons for open volume (they are much more sensitive than electrons in electron microscopy), positron annihilation spectroscopy (PAS) and especially positron beam analysis (PBA) has developed over the last few decades into a successful non-destructive method for probing low atomic density regions (e.g., vacancies, clusters of vacancies, and nanocavities) in materials over a wide range of depths, from the surface to depths of hundreds of nanometers. For a review reference is made to [8,9].

2. Experimental

In order to create nanoclusters monocrystalline MgO(1 0 0) samples were sequentially implanted with 1×10^{16} Cd and 1×10^{16} Se ions cm^{-2} at an energy of 280 and 210 keV, respectively. After ion implantation isochronal annealing was performed in ambient air at temperatures up to 1500 K in steps of 200 K for periods of 0.5 h. After ion implantation and after each annealing step, the defect evolution in the sample was monitored using optical absorption spectroscopy and Doppler broadening positron beam analysis (PBA) [8,9]. The optical absorption measurements were performed using a Perkin–Elmer Lambda 40 spectrophotometer. For the PBA experiments, a mono-energetic positron beam with a variable energy of 0–30 keV was used. A few samples were examined by means of cross-sectional transmission electron microscopy (XTEM) after the 1300 K annealing step. The specimen preparation is discussed elsewhere [10]; the microscope used was a JEOL 4000 EX/II operating at 400 kV (point-to-point resolution 0.165 nm).

3. Results and discussion

The ion implantation energies were chosen in such a way that the Cd and Se ion implantation profiles overlap as much as possible. Fig. 1 shows the SRIM calculations [11] for 280 keV Cd and 210 keV Se. Displacement energies of 55 eV were used for both the Mg and the O atoms [12]. As is clear from the figure, the straggling of the Se profile is somewhat larger than that of the Cd profile. However, during the nanocluster formation process, the atoms are somewhat mobile, which is expected to reduce a possible deviation from stoichiometry, which is very limited for bulk CdSe [13]. Cd and Se have melting points

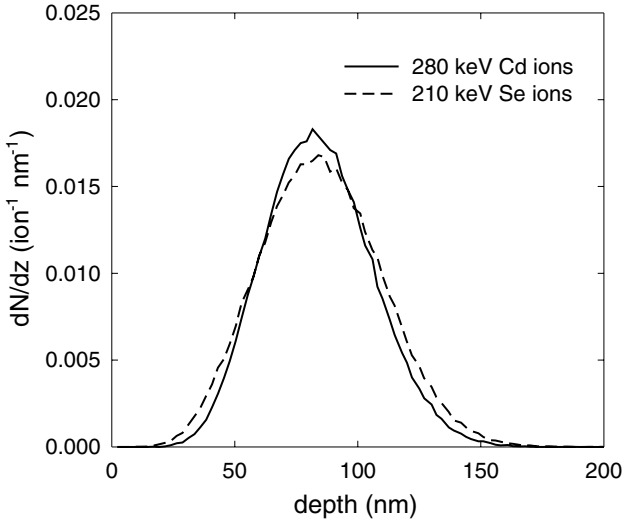

Fig. 1. Predicted depth distribution of 280 keV Cd ions and 210 keV Se ions in MgO, calculated with the SRIM code [11]. For both distributions, the number of calculated ion tracks is 100,000.

(594 and 490 K, respectively), which are much lower than that of CdSe (1350 K [14]). Cd and Se nanoclusters will therefore be less stable during thermal annealing and will easily dissociate to form CdSe nanoclusters, in particular because a large reduction in Gibbs-free energy is associated with the formation of CdSe from its pure constituents [13]. At the peak of the CdSe distribution, the concentration is 3.2 mol% (CdSe per MgO).

Fig. 2 shows the optical absorption spectra after ion implantation and after various annealing steps. After ion implantation, V-centres (Mg monovacancies) are

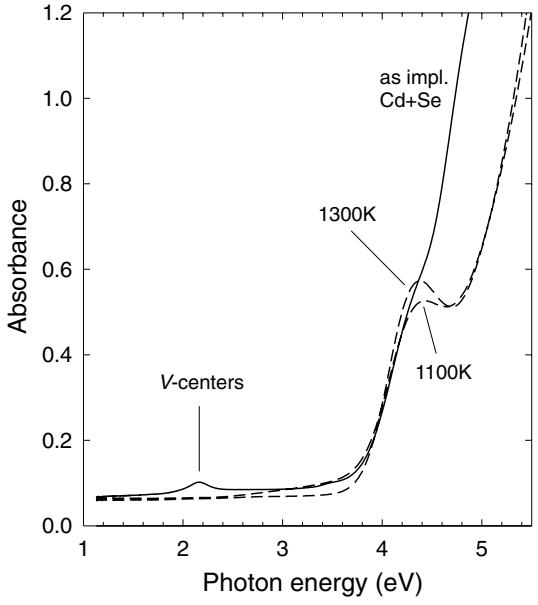

Fig. 2. Optical absorption spectra of MgO as-implanted with Cd and Se and after annealing at the indicated temperatures.

present at a photon energy of 2.2 eV, as well as F-centers (O monovacancies) at an energy of 4.9–5.0 eV. After annealing at 700 K, an absorption peak appears at 4.4 eV corresponding to Fe^{3+} impurity centers [15]. Fe is a common impurity atom in MgO crystals. During the annealing procedure the V-centers dissociate and the intensity of the F-centers reduces. Unfortunately no evidence of CdSe nanoclusters can be found in the optical absorption spectra. These could be expected at a band gap energy in the range of 1.8–2.5 eV. It is not likely that the absorption peak at 2.2 eV in Fig. 2 corresponds to CdSe nanoclusters (instead of V-centers), because this peak disappears already after annealing at a temperature of 500 K. The broad size distribution and the different crystal structures of the CdSe nanoclusters created with ion implantation (see the discussion of the TEM results below) will give a smeared absorption band originating from a multitude of absorption peaks rather than one or more distinct absorption peaks. The position of the peak depends on the size (and therefore the band gap) of the nanocluster. For example, nanoclusters with a size of 2 nm give an absorption peak at ~2.5 eV while nanoclusters with a size of 4 nm produce an absorption peak at ~2.1 eV [3]. Nevertheless, despite the size dispersion, it is possible to detect optical absorption by CdSe nanoclusters when the number of nanoclusters is sufficiently high. In a previous study, CdSe nanoclusters were created by means of ion beam synthesis in sapphire Al_2O_3 [6] where an absorption edge was found at a wavelength of ~700 nm, corresponding to a band gap of ~1.8 eV. Recently, the absorption edge of wurtzite CdSe was also found in an MgO sample implanted with very high doses of Cd and Se (peak concentration 15 mol%) [16]. In the present work the ion implantation doses are much lower (peak concentration 3.2 mol%) indicating that the overall intensity generated by the nanoclusters is too low to be resolved.

Fig. 3 shows the *S* parameter (indicator of open-volume defects) as a function of positron implantation energy. The average positron implantation depth is indicated at the top of the figure. It should be realized that the depth resolution is limited due to the straggling of the positron implantation profile and positron diffusion processes (the resolution is approximately 20% of the implantation energy). In order to facilitate the discussion, a four-layer model is indicated in the figure. Layer I contains mostly displacement damage, layer II is the ion implantation range, layer III is a 'tail' of implantation defects mainly caused by channelling effects, and layer IV is the MgO bulk. The boundaries of layer II correspond reasonably well to the ion range predicted by SRIM in Fig. 1. Directly after ion implantation, the *S* parameter in layers I–III increases due to the creation of vacancies and vacancy clusters.

During the subsequent annealing steps, the *S* parameter increases further because of the growth of vacancy

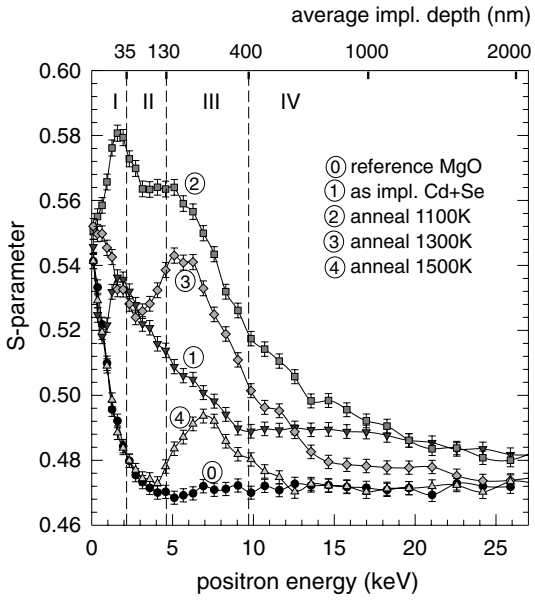

Fig. 3. *S* parameter as a function of positron implantation energy for the MgO sample as-implanted with Cd and Se and after annealing at various temperatures. The average positron implantation depth is indicated at the top of the figure.

clusters until a maximum in the *S* parameter is reached after annealing at 1100 K. At higher temperatures, the *S* parameter decreases in layers I–III because of shrinkage and dissociation of vacancy clusters. Considering the *S* parameter curve after annealing at 1300 K, it is clear that the *S* parameter in layer II (ion implantation range) has become lower than in layers I and III (containing mostly implantation damage). Undoubtedly, layer II also contains implantation damage but in this layer the vacancy-type defects recombine with the implanted Cd and Se ions so that there are fewer open-volume defects to trap the positrons. The result is a low *S* parameter in layer II (in comparison to the adjacent layers) after annealing at 1300 K. After annealing at 1500 K, the *S* parameter in layers I–III reduces even further.

TEM analysis was performed on a cross-section of a sample after the 1300 K annealing step. CdSe nanoclusters with size-dependent structural properties were found with sizes ranging from a few to 20 nm, but rarely even larger clusters of 40–50 nm were observed. There are three different crystal structures of CdSe: halite (cubic, rock-salt), sphalerite (cubic, zinc-blende) and wurtzite (hexagonal) [4,8]. The lattice parameters of the three crystal structures are given in Table 1. Wurtzite is the most stable structure for CdSe in bulk form at room temperature; sphalerite is slightly less stable. The lattice parameter for rock-salt CdSe is deduced from the work of Jacobs et al. [8]. Although the value of the lattice parameter is not mentioned explicitly in this work, it can be deduced from the X-ray diffraction data. The (2 0 0) peak of rock-salt CdSe has a centroid at $Q = 2\pi/d_{200} = 2.24$ Å^{-1} so that $a_{CdSe} = 5.61$ Å. This value does not refer to bulk CdSe, but to CdSe nanoclusters with a size of 11 ± 1 nm and at a pressure of 9 GPa.

In the high-resolution image of Fig. 4, three small CdSe nanoclusters can be observed. Translational moiré fringes were observed to run in both the MgO[0 1 0] and the MgO[0 0 1] directions for all nanoclusters with a size less than 5 nm. This shows that the CdSe crystal structure is cubic. The lattice parameter can be deduced from the spacing of the moiré fringes, using the following relationship:

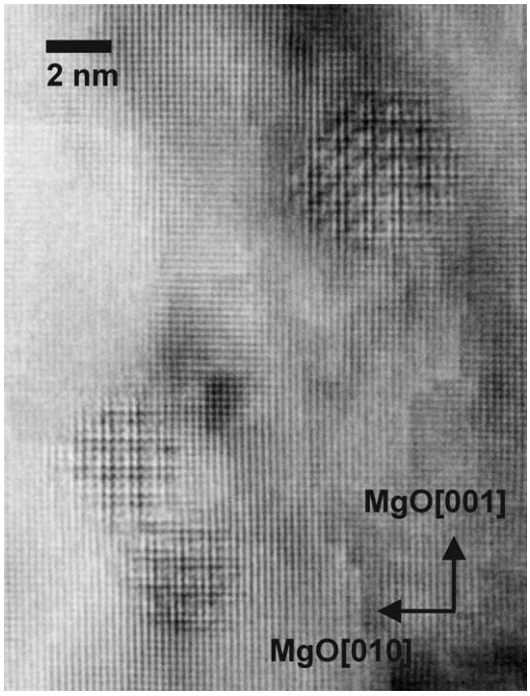

Fig. 4. High-resolution TEM image of small (<5 nm) CdSe nanoclusters with a rock-salt crystal structure, showing translational Moiré fringes in both the MgO[0 0 1] and MgO[0 1 0] directions.

Table 1
Crystal structures and lattice parameters of MgO and CdSe

Material	Structure	Type		Lattice parameters (Å)	V_{mol} (Å^3)	Reference
MgO	Rock-salt	Halite	Cubic	*a*: 4.213	18.7	[19]
CdSe	Rock-salt[a]	Halite	Cubic	*a*: 5.61[a]	44.1	[8]
	Zinc blende	Sphalerite	Cubic	*a*: 6.077	56.1	[19]
	Zincite	Wurtzite	Hex.	*a*: 4.298	56.0	[19]
				c: 7.002		

[a] For CdSe nanoclusters at a pressure of 9 PGa.

$$\frac{1}{d_{\text{fringes}}} = \left| \frac{1}{d_{\text{MgO}}} - \frac{1}{d_{\text{CdSe}}} \right|. \qquad \text{(OR1)}$$

MgO has a lattice parameter of 4.213 Å so that $d_{\text{MgO}(002)} = 2.107$ Å. From Fig. 4, it is clear that there are exactly four MgO fringes per moiré fringe. This means for CdSe that $d_{\text{CdSe}} = 4/3 \cdot d_{\text{MgO}(002)} = 2.81$ Å. Table 1 gives a lattice parameter of rock-salt CdSe of 5.61 Å so that $d_{\text{CdSe}(002)} = 2.81$ Å, which coincides with the value calculated from the moiré fringes. From the observations above it is also clear that the clusters are in a cube-on-cube orientation relationship with the MgO host (OR 1). Rock-salt CdSe is more ionic than sphalerite or wurtzite CdSe so that it fits better into the ionic MgO lattice. Moreover, the smallest nanoclusters experience the largest pressure, and rock-salt CdSe is more densely packed than the other structures. The molecular volume of rock-salt CdSe is 21% smaller than the molecular volume of the sphalerite or wurtzite phase (see Table 1). This explains why the smallest clusters prefer to have the rock-salt structure despite the very large lattice mismatch with MgO of 33% (calculated as $(d_{\text{CdSe}} - d_{\text{MgO}})/d_{\text{MgO}}$).

Fig. 5 shows three CdSe nanoclusters with sizes of 5–10 nm with a structure clearly deviating from the rock-salt one. Here moiré fringes and high-resolution interference patterns are observed. In the TEM image of Fig. 6, a number of small rock-salt CdSe nanoclusters can be observed, together with a larger CdSe nanocluster with clear lattice fringes not distorted by moiré fringes. In this projection direction, the image of the large cluster can correspond with wurtzite or sphalerite CdSe. In Fig. 7, HRTEM Image simulations (MacTempas) are shown of sphalerite viewed along [1 1 2] and wurtzite viewed along $[10\bar{1}0]$. Here a thickness of 6.3 nm was used for the sphalerite phase and 6.1 nm for the wurtzite phase. At a defocus of −12 nm, the simulations yield identical HRTEM images that perfectly match the observed structure in Fig. 6. Thus, the clusters with size larger than 5 nm have the sphalerite or the wurtzite crystal structure. In the case of sphalerite, the orientation relationship is

$$(2\bar{2}0)_s // (020)_{\text{MgO}}, \quad [11\bar{2}]_s // [100]_{\text{MgO}}, \qquad \text{(OR2)}$$

which also implies $(111)_s // (002)_{\text{MgO}}$. In the case of wurtzite it is

$$(1\bar{2}10)_w // (020)_{\text{MgO}}, \quad [10\bar{1}0]_w // [100]_{\text{MgO}}, \qquad \text{(OR3)}$$

which also implies$(0002)_w // (002)_{\text{MgO}}$.

To allow the distinction between these two CdSe phases, another viewing direction is needed. This is the case in Fig. 8 for an even larger cluster than in Fig. 6; here the partly shown precipitate has a size of about 40 nm. The *d*-spacings and symmetry present in the lattice image of the CdSe in Fig. 8 unambiguously match with the one of the wurtzite structure as viewed along $\langle 01\bar{1}1 \rangle$. However, this wurtzite cluster thus shows another orientation relation with the MgO than specified by OR 3. According to Fig. 8 it holds:

$$(1\bar{2}10)_w // (020)_{\text{MgO}}, [10\bar{1}1]_w // [100]_{\text{MgO}}, \qquad \text{(OR4)}$$

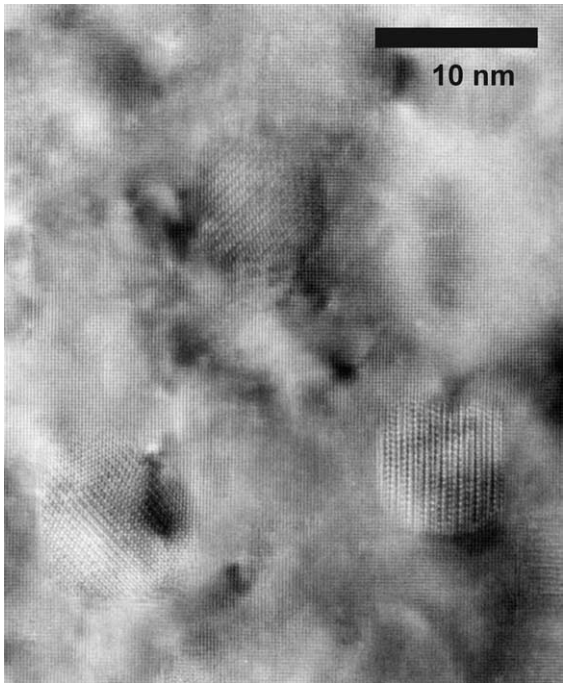

Fig. 5. High-resolution TEM image of three CdSe nanoclusters in the size range of 5–10 nm. The clusters have either the sphalerite or wurtzite structure.

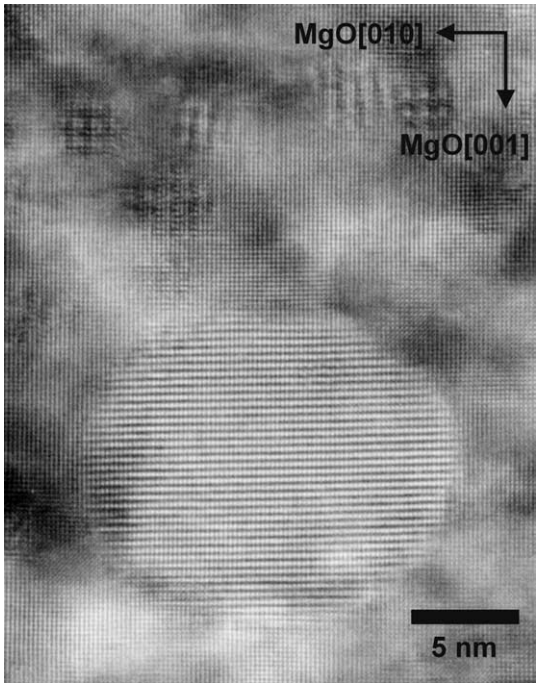

Fig. 6. HRTEM image with a number of small rock-salt CdSe nanoclusters at the top and a very large CdSe nanocluster at the bottom of the figure. The strong fringes in the large nanocluster are not Moiré fringes but CdSe lattice fringes from either sphalerite or wurtzite.

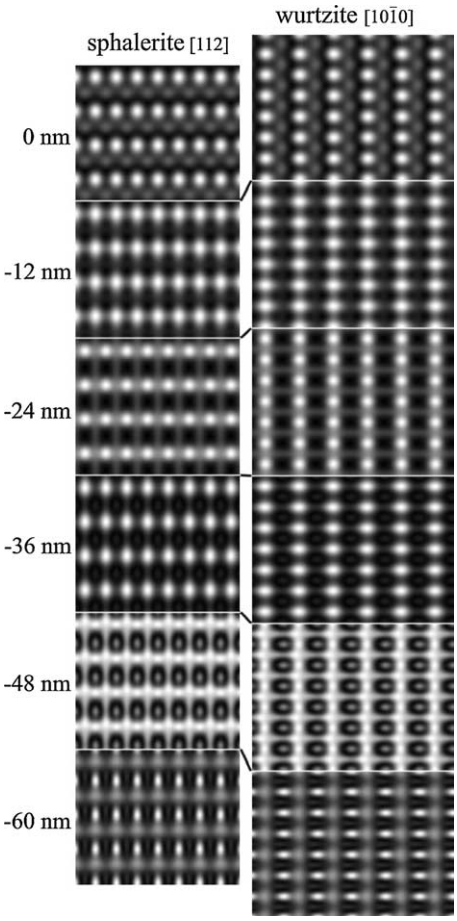

Fig. 7. Simulated HRTEM images of [1 1 2] sphalerite and [10$\bar{1}$0] wurtzite. The numbers on the side designate the defocus in nm. Both phases at a defocus of −12 nm match exactly with the image of the large CdSe cluster in Fig. 6.

which also implies$(\bar{1}012)_w//(002)_{MgO}$. Both OR 3 and OR 4 are characterized by nearly strain-free matching of $(1\bar{2}10)$ planes on the (0 2 0); difference in *d*-spacing is only 2.1%. This is of course much less than the 33% that existed between rock-salt CdSe and MgO. OR 3 and OR 4 are closely related by a mutual rotation of the CdSe with 39.2° around the common normal of the$(1\bar{2}10)$ plane where the two lowest index planes of CdSe parallel to cube planes of MgO in OR 3 are replaced by the next two lowest index planes (i.e., 3 and 4) of CdSe in OR 4. Another typical feature of OR 3 is that 3 (0 0 0 2) CdSe planes excellently match 5 (0 0 2) MgO planes.

Now returning to Fig. 5 the CdSe precipitates there can be identified using the knowledge obtained for the larger clusters which do not suffer from confusing moiré effects. The one on the lower right shows clearly OR 3 (or OR 2). Considering the horizontal spacing between the fringes, it is clear that 3 (0 0 0 2) CdSe planes match 5 (0 0 2) MgO planes. The two other precipitates show OR 4. Particularly, this last type cannot be identified directly, because is obscured by the general moiré (both translational and rotational) present. So, the main conclusion is that clusters with a size larger than 5 nm adopt the wurtzite crystal structure with two possible orientation relations as specified by OR 3 and OR 4. Large clusters must have the wurtzite structure. Of course the statistics are insufficient to exclude that sphalerite precipitates exist for intermediate cluster sizes (above 5 nm), but taking the present observations into account this is unlikely. Note that the present results imply that, if mono-disperse CdSe clusters in MgO are created (in sufficient numbers), a clear distinction in the band gap (both in size and direct/indirect character) and, e.g., the related optical properties must be present for cluster sizes above or below 5 nm [4,16].

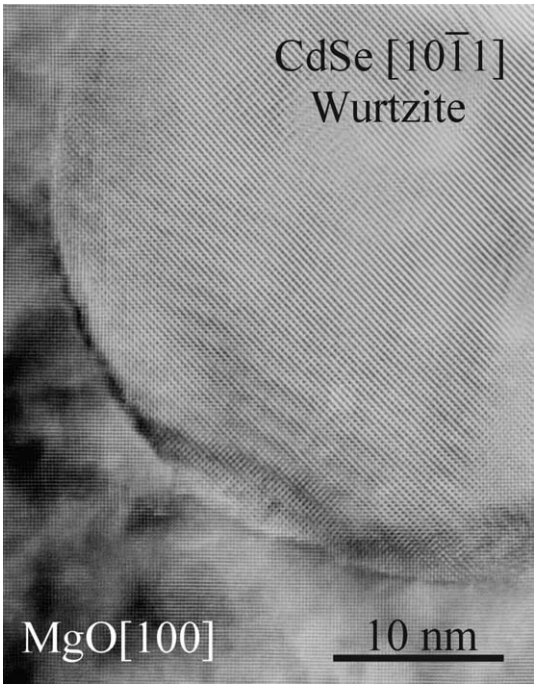

Fig. 8. HRTEM image of a large CdSe cluster with the wurtzite structure as viewed along $[10\bar{1}1]_w//[100]_{MgO}$.

Considering the morphology of the nanoclusters, the larger monoclusters in Figs. 6 and 8 are spherical by approximation while the smaller nanoclusters in Fig. 5 are more faceted. Apparently, the size ratio of the various facets changes with the cluster size. The small nanoclusters (<10 nm) are more cubic because of relatively large MgO{1 0 0} facets. The size ratio of the facets is directly related to the interface energy of the facets (the lower the interface energy, the larger the facet), which can be quite different for polar and non-polar surfaces of MgO. The MgO{1 0 0} and MgO{1 1 0} surfaces are non-polar. The MgO{1 1 1} surface is polar and unless reconstructed is unstable as a free surface [10,17]. However, the oxygen terminated MgO{1 1 1} facet is the energetically most favourable when there is an interface with metal particles, such as Cu precipitates in MgO [18]. Here image charges in the metal compensate for the electric dipole at the interface. CdSe is a semiconductor and is much less able to create image charges. For the smallest precipitates, the CdSe

crystal is so small that image charges are hardly formed and this renders a high formation energy of the polar {1 1 1} interface. This explains why the {1 0 0} facets are dominant for the small clusters of Fig. 5. The large clusters in Figs. 6 and 8 are large enough to create image charges, thus allowing the presence of polar interfaces. The large clusters are therefore more spherical.

4. Conclusions

CdSe nanoclusters were successfully created in MgO by means of ion beam synthesis with post-implantation thermal annealing at 1300 K. After this anneal, the CdSe nanoclusters have a broad size distribution typically in-between 2 and 20 nm with rare extremes of about 40 nm. No optical absorption peaks could be found that could be attributed to CdSe due to a too low number of nanoclusters to cause significant absorption. The clusters smaller than 5 nm have the rock-salt crystal structure and are in a cube-on-cube orientation relationship with the MgO host matrix. Nanoclusters larger than about 5 nm have the wurtzite crystal structure and were observed to have two different orientation relations with the MgO. The confinement by the host MgO and the size-dependent internal pressure within the CdSe nanoclusters are responsible for the, from the stable bulk wurtzite deviating, rock-salt structure of the clusters smaller than 5 nm.

Acknowledgements

The authors are grateful to professor A. van Veen, who contributed greatly to the success of this work. Professor A. van Veen deceased on January 3, 2004.

References

[1] Kamat PV, Meisel D, editors. Semiconductor nanoclusters. New York: Elsevier; 1997.
[2] Goldstein AN, Echer CM, Alivisatos AP. Science 1992;256:1425.
[3] Alivisatos AP. Science 1996;271:933.
[4] Alivisatos AP. J Phys Chem 1996;100:13226.
[5] Peng X, Manna L, Yang W, Wickham J, Scher E, Kadavanich A, et al. Nature 2000;404:59.
[6] White CW, Budai JD, Withrow SP, Zhu JG, Sonder E, Zuhr RA, et al. Nucl Instrum Meth Phys Res B 1998;141:228;
White CW, Budai JD, Withrow SP, Zhu JG, Sonder E, Zuhr RA, et al. Nucl Instrum Meth Phys Res B 1999;148:991.
[7] Jacobs K, Wickham J, Alivisatos AP. J Phys Chem B Lett 2002;106:3759.
[8] van Veen A, Schut H, Mijnarends PE. In: Coleman P, editor. Positron beams and their applications. Singapore: World Scientific; 2000. p. 191 [Chapter 6].
[9] De Hosson JThM, van Veen A. In: Nalwa HS, editor. Encyclopedia of nanoscience and nanotechnology, vol. 7. CA, USA: American Science Publishers; 2004. p. 297–349.
[10] Kooi BJ, van Veen A, De Hosson JThM, Schut H, Fedorov AV, Labohm F. Appl Phys Lett 2000;76:1110.
[11] Ziegler JF, Biersack JP, Littmark U. The stopping and range of ions in solids (TRIM). New York: Pergamon; 1985. Available from: <www.srim.org> for information on updated versions.
[12] Zinkle SJ, Kinoshita C. J Nucl Mater 1997;251:200.
[13] Barin I. Thermochemical data of pure substances. Weinheim: VCH; 1993.
[14] Handbook of chemistry and physics, 66th ed. USA: CRC Press; 1986.
[15] Las WC, Stoebe TG. Radiat Prot Dosim 1984;8:45.
[16] Eijt SWH, van Huis MA, Mijnarends PE, Kooi BJ, Nanu M. MRS 2004 Fall Meeting Conf. Proc [submitted].
[17] Watson GW, Kelsey ET, de Leeuw NH, Hams DJ, Parker SC. J Chem Soc Faraday Trans 1996;92:433.
[18] Backhaus-Ricoult M. Acta Mater 2001;49:1747.
[19] JCPDS Database file 04-0829 (for MgO), file 19-0191 (for sphalerite CdSe) and file 08-0459 (for wurtzite CdSe), International Centre for Diffraction Data.